

PIPELINES INSPECTION USING MAGNETIC INDUCTION TOMOGRAPHY BASED ON A NARROWBAND PASS FILTERING METHOD

L. Ma, H.-Y. Wei, and M. Soleimani

Department of Electronic and Electrical Engineering, University of Bath, UK

Abstract—Pipelines are the most common apparatus in industries; therefore, the need for inspection during the manufacturing, construction and the operation stage is inevitable and invaluable. Magnetic Induction Tomography (MIT) is a new type of tomography technique that is sensitive to the electrical conductivity of objects. It has been shown that the MIT technique is appropriate for imaging materials with high electrical conductivity contrasts; hence, the majority of the MIT systems were designed for detecting metallic objects. In this paper, MIT technique was proposed for pipeline inspection. Structural damages of the outer surface of the pipe were considered in this study. Nonetheless, it is challenging to use the traditional MIT pixel based reconstruction method (PBRM) as a suitable pipelines inspection tool because of the limited resolution. A narrowband pass filtering method (NPFM) of imaging pipe geometry was developed as a suitable image reconstruction method. The proposed method can overcome the resolution limitations and produce useful information of the pipe structure. This paper shows the comparative results from the novel NPFM and from traditional PBRM. While the PBRM fails to detect damages in outer structure of the pipe the NPFM successfully indentifies these damages. The method has been verified using experimental data from very challenging test samples. It is well known that using a coil array with an imaging region of 100 mm the PBRM based MIT can retrieve information with accuracy of about 10 mm (about 10%). With proposed NPFM the information on a resolution of 2 mm (which is about 2%) can be detected using the same measurement data.

Received 11 November 2011, Accepted 5 January 2012, Scheduled 8 January 2012

* Corresponding author: Manuchehr Soleimani (m.soleimani@bath.ac.uk).

1. INTRODUCTION

Eddy current techniques are widely used for inspecting metallic structures. When the metal conductor is exposed to the changing magnetic field (caused by the alternating current), the eddy current is induced in the conductor. Magnetic induction tomography (MIT) is a new tomography technique that utilizes this eddy current measurement [1, 4–6, 8]. The fundamental principle of the MIT is as follows: by passing a sinusoidal signal through an excitation coil, it can produce a primary magnetic field that induces the eddy current. This eddy current can then generate the secondary magnetic field that can be detected by sensing coils. Since the properties of the secondary magnetic field depend on the material's property, analyzing this detected secondary field can provide information about the material. It should be noted that MIT is not only sensitive to conductivity, but also the other two passive electromagnetic properties: permeability [10, 13] and permittivity. MIT is a member of low frequency electrical and electromagnetic tomography [14–16]. In this paper, a novel narrowband pass filtering method (NPFM) was applied in MIT system to realize the pipeline inspection process. Several experiments were carried out to investigate the feasibility of this novel method using analysis of the singular values, image visualization, and analyzing the measured voltages. The NPFM method was compared to the traditional pixel based reconstruction method (PBRM) and significant improvement was achieved. The imaging of the outer surface of the pipe is the main aim of this study. If successful, the MIT can provide a valuable structural health monitoring for pipelines and in particular for pipes covered under claddings.

2. MIT SYSTEM FOR PIPELINE IMAGING

Our MIT system consists of (i) an array of equally spaced inductive coils arranged around the object periphery, (ii) an National Instrument data acquisition system and (iii) a host computer; as shown in Figure 1. Eight 50 turns air-core coil were constructed manually to form a 100 mm diameter-imaging region. One of the eight inductive coils is supplied with an alternating current of 5 mA and the operational frequency is 20 kHz. The working frequency is higher than other metallic MIT systems [7], this is because we intend to study the outer surface of the pipe. Due to the skin effect, the higher frequency excitation will provide higher sensitivity in exterior surface and becomes less sensitive to internal structures. The choice of frequency becomes more crucial when inspection of inner part of the metallic pipe

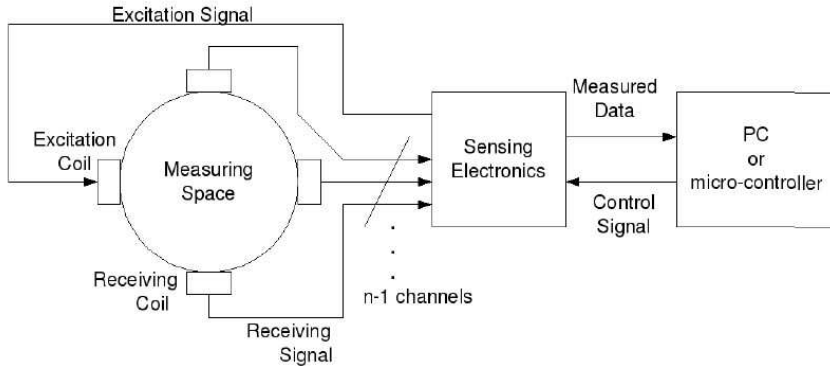


Figure 1. MIT system architecture.

to be considered. An ADG406 multiplexer is engaged in the system to accomplish the channel switching process, ADG406 is a monolithic CMOS analog multiplexer which has a low power dissipation, high switching speed and low on resistance advantages. These features make the chip suitable for developing a high-speed data acquisition system. Each channel conducts equally well in both directions as long as the device is enabled and has an input signal ranges within the supplies. All channels exhibit break-before-make switching action preventing momentary shorting when switching channels. It is worth noticing that the MIT system presented in this paper uses only eight multiplexer channels during the channels switching process, this indicates the existing MIT system can be further expanded to sixteen channels to enhance the full capacity of the ADG406 multiplexer. An NI USB-6295 data acquisition device is used to interface between the ADG406 multiplexer and a host PC. The aim of the device is to collect individual data efficiently, combine data effectively and display data in images to suit the need for real-time monitoring. For eight channels MIT system, there are 28 unique coil pairs. 1-2, 1-3, ..., 1-8, 2-3, 2-4, ..., 7-8, giving 28 independent measurements. The image reconstruction module extracts 28 independent measurements to perform the reconstruction algorithm, displays and updates the images. The signal to noise ratio in this MIT system is between 50 dB (for measurement between two opposite coils) and 70 dB (for measurement between two neighboring coils), which is comparable with similar MIT systems [7]. The material of the experimental pipe samples is aluminium which has conductivity of $3.5 \times 10^7 \text{ S}\cdot\text{m}^{-1}$.

3. IMAGE RECONSTRUCTION

The MIT image reconstruction problem is a challenging ill-posed inverse problem [12, 16–19]. *A priori* information is the key to successful reconstruction process. In pipe imaging, there is geometrical *a priori* knowledge that will be fully explored in our NPFM.

For an electromagnetic tomography imaging system, two problems have to be solved, namely the forward and inverse problems. Given the distribution of conductivity (or other passive electromagnetic properties) with excitation current, the forward model is to solve the estimated measurement signals from the sensors. In MIT the forward problem is referred as eddy current problem in terms of Maxwell's equations and can be solved numerically using a technique such as the finite element method (FEM). On the contrary, the inverse problem is to solve the distribution of conductivity (or the other passive electromagnetic properties) while the measurement signals are given. Inverse algorithm usually makes use of the forward model as part of the solving process. For MIT system, by computing the measured changes between mutual inductance, the distribution of the conductivity can be reconstructed; the characteristics of the conductor can also be analyzed through the distribution of the conductivity.

The forward problem in MIT is a classical eddy current problem [3]. This problem can be formulated in terms of the magnetic vector potential A for the sinusoidal waveform excitation cases using complex phasor notation

$$\nabla \times \left(\frac{1}{\mu} \nabla \times A \right) + i\omega\sigma A = J_s \quad (1)$$

where σ is electrical conductivity, μ is magnetic permeability and J_s is the applied current density in an excitation coil. In this study we used magnetic vector potential A , A formulation for the eddy current problem. If the total current in the excitation coil was I_0 , the sensitivity [2], [11] of the induced voltage to the conductivity change is

$$\frac{\partial V_{mn}}{\partial \sigma_k} = -\omega^2 \frac{\int A_m \cdot A_n dv}{I_0} \quad (2)$$

where V_{mn} is the measured voltage, σ_k is the conductivity of pixel k , Ω_k is the volume of the perturbation (pixel k), A_m and A_n are respectively solutions of the forward problem when excitation coil (m) is excited by I_0 and sensing coil (n) is excited with unit current. The linear image reconstruction method is based on Tikhonov regularization, which uses a universal regularization technique for solving the ill-posed inverse

problem in the following manner:

$$x = (J^T J + \lambda I)^{-1} J^T z \tag{3}$$

where x is the image pixel vector and z the measurement vector. Here, J is the sensitivity matrix (Jacobian matrix), I an identity matrix and λ the regularization parameter. A difference-imaging mode was used, in which the measured data z is the difference between the latest measurement and a reference measured data. In difference imaging mode the image x is also a difference between the latest position of the object and the reference position. In PBRM the x includes all pixels in imaging region. In this single-step algorithm, sensitivity matrix, J , was obtained from the result of the forward model and using Equation (2). A nonlinear image reconstruction method will give a more accurate account of the object, but will involve re-calculation of the forward problem and the Jacobian matrix. The MIT system presented in this work manipulates 28 measurements to reconstruct images. The pixel mesh grid is 41 by 41.

3.1. Narrowband Pass Filtering Method

The PBRM is a searching algorithm looking for the best fit of imaging values to create an estimated measured data that matches the real measurement. In PBRM, the imaging domain is divided into small elements by equally spaced 1681 pixels in cartesian coordinate system; however, not all the pixels are presenting useful information in the imaging domain for our pipe imaging. In NPFM, the pixels in cartesian

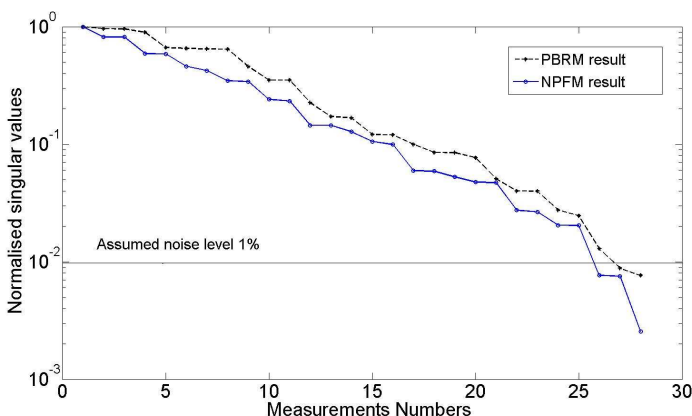


Figure 2. Singular values plots for PBRM and NPFM.

coordinate system have been transferred and then filtered in polar coordinate system. It is important to notice that only the pixels in the region of interest (ROI) contribute to the final inversion algorithm. Figure 2 shows the singular value decomposition for both NPFM and PBRM. In the 100 mm imaging region, PBRM employs 41 by 41 uniformed pixels located in x axis and y axis from the cartesian coordinate system which generates 26 singular value above an assumed 1% noise level. As the sample pipe is placed in the centre and it does not occupy the whole imaging region, therefore the 26 singular values are partially wasted which means the number of singular values that contributes to the final image in pipe region is less than 26. The NPFM accomplished a tradeoff between compensating singular values by discarding redundant pixels that are not in the ROI. The result of implementing the NPFM is that 1125 pixels have been excluded from the imaging domain, leaving 556 pixels to reconstruct the final image. As consequences, the 25 singular values that are above the noise level are fully employed in the image reconstruction. The result of using NPFM is the search area is limited to the area of pipe, which improves the resolution of reconstructed images. For the same noise level more information can be extracted using NPFM as the number of unknown are smaller for the same number of singular values above a given noise level [9]. This can be seen in Figure 3, the Figure 3(c) (NPFM) gives a better reflection of the characteristics of the sample than Figure 3(b). The NPFM has produced an image reflecting the shape of the pipe taking advantage of targeted region of interest (ROI) for the imaging. Note that in example of Figure 3 the narrowband region was selected to be exactly the same size as the pipe. This choice is suitable if we know that the centre of pipe matches that of the exact centre of the coil array. In practical term, assuming a larger ROI will allow to compensate any mismatch between the actual centre of the pipe and the centre of the coil array.

The measured voltage data will be the same for PBRM and NPFM, therefore any resolution improvement achieved is due to the filtering process. The imaging domain will be transferred from (x, y) cartesian coordinate system to (r, θ) polar coordinate system. It is important to remind that only r component of the imaging domain has been filtered by defining the estimated location of pipe sample in terms of inner radius r_i and outer radius r_0 .

4. THE INSPECTION OF PIPELINES

There are several pipeline inspection techniques available for industrial purposes. However, those techniques require direct contact with

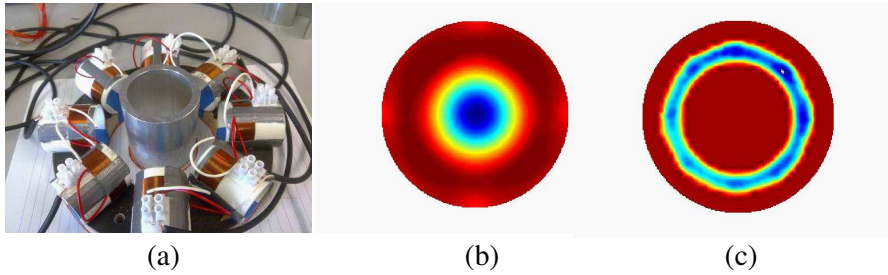


Figure 3. (a) True sample. (b) PBRM result. (c) NPFM result.

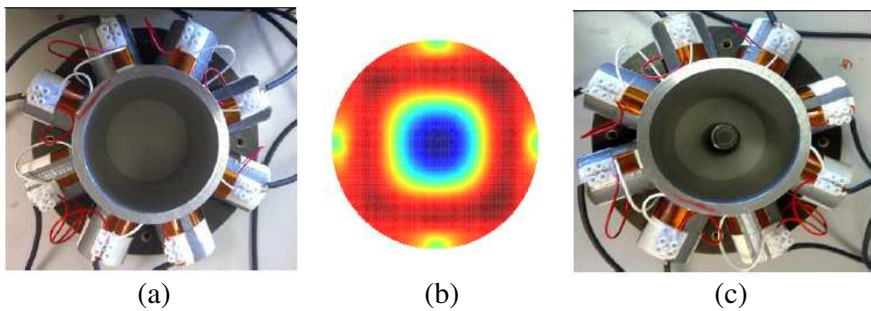


Figure 4. (a) Tube inspection and reconstructed image. (b) Reconstruction of both cases. (c) Tube with and without a metal object in centre.

pipelines in order to carry out the investigation. Here, we propose the non-destructive and contactless MIT technique for pipeline inspection, especially for the pipeline covered by non-conductive claddings. Moreover, MIT is a technique only sensitive to high conductivity materials, which means that the inspection can be achieved without removing the claddings. This is a major advantage of the MIT for the pipeline imaging applications. Figures 4(a) and 4(b) show the image of the pipe sample with and without an extra conductive object presented inside the pipe respectively. Figure 4(b) demonstrates that the metal object placed inside the pipe has negligible impact on the reconstructed image, which means that the inspection of the exterior surface of the pipe can be carried out without being effected by the material flowing inside the pipeline.

Furthermore, for the pipeline inspection application, we are only interested in imaging the pipeline area (which is in a cylindrical shape). In addition to that, we are focusing on the outer surface of the pipe



Figure 5. Demonstration of the concept of narrow band-pass region.

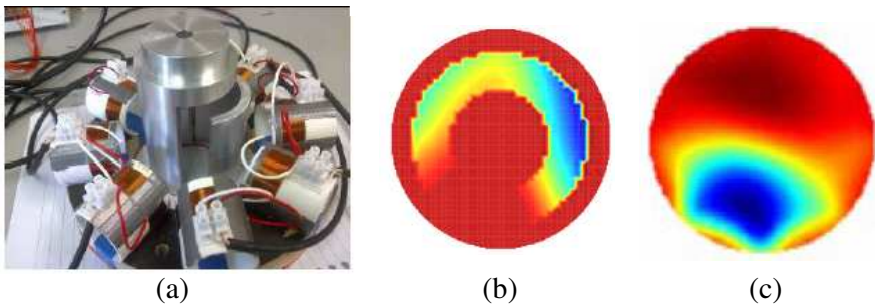


Figure 6. (a) Pipe with large opening. (b) Reconstructed image using NPFM. (c) Reconstructed image using PBRM.

in this study. Figure 5 shows the narrowband pass region used for the rest of the pipeline experiments in this paper. In practical term, this was chosen to be slightly larger than the pipe itself. This ensures that the pipe will be covered in the narrowband if the centre of pipe is not exactly in the center of coil array.

Figure 6 shows reconstruction of a large opening in damaged pipe geometry. This is not a challenging task for pipe inspection, but can represent the potential use of the MIT method for broken pipes for example for underwater pipeline inspection.

To show the capability of the proposed NPFM technique to identify the opening of the pipe, several tests have been carried out. Figure 7 shows the reconstruction of various samples with different sizes of opening. Figure 7 shows an opening of 0, 10, 45, and 90 degrees, respectively for various metallic samples. Experiments of Figure 7 are done by free space measured data as background and with exact size of the pipe as narrowband.

The following experiments are aiming to simulate the detection of

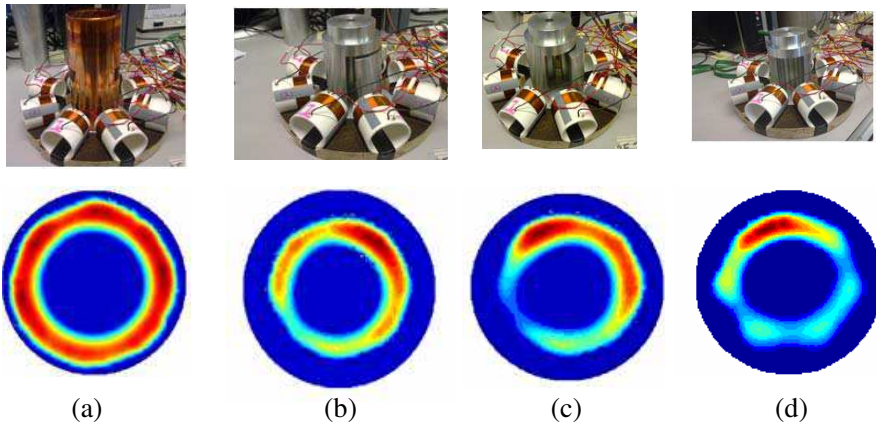


Figure 7. (a) Full pipe. (b) Small opening. (c) Large opening. (d) Half circle.

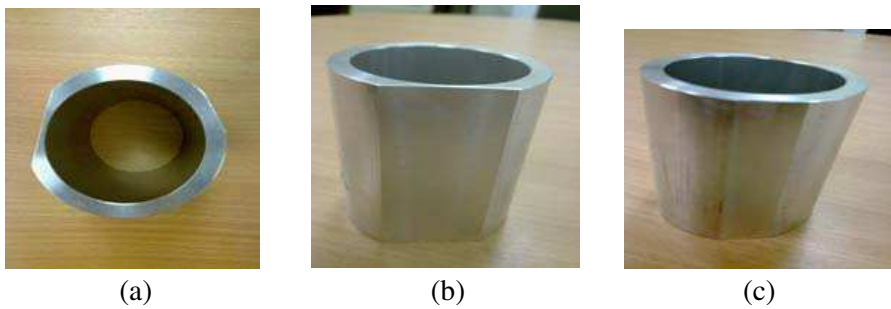


Figure 8. Damaged pipe conditions.

the damages on the outer surface of the pipe. Figure 8(a) shows a top view of an aluminium pipe with an inner radius of 25.5 mm and the outer radius of 31.5 mm, therefore the thickness of the pipe is 6 mm. As it can be seen, there are two damages on the outer surface. The large damage as shown in Figure 8(b) has a thickness of 1.62 mm and the smaller damage as shown in Figure 8(c) has a thickness of 4.95 mm.

Figure 9 shows challenging test samples using both PBRM and NFRM. In the left hand side (9(a)), a complete cylindrical pipe can be seen. In the middle (9(b)), a large cut has been applied to the surface of cylinder, the same as Figure 8(b). Right hand side (9(c)) shows a large cut and a small cut to the surface of the pipe, the small cut is the same as Figure 8(c). The proposed NFRM shows successful inspection results in all these cases. The PBRM would fail in all these cases.

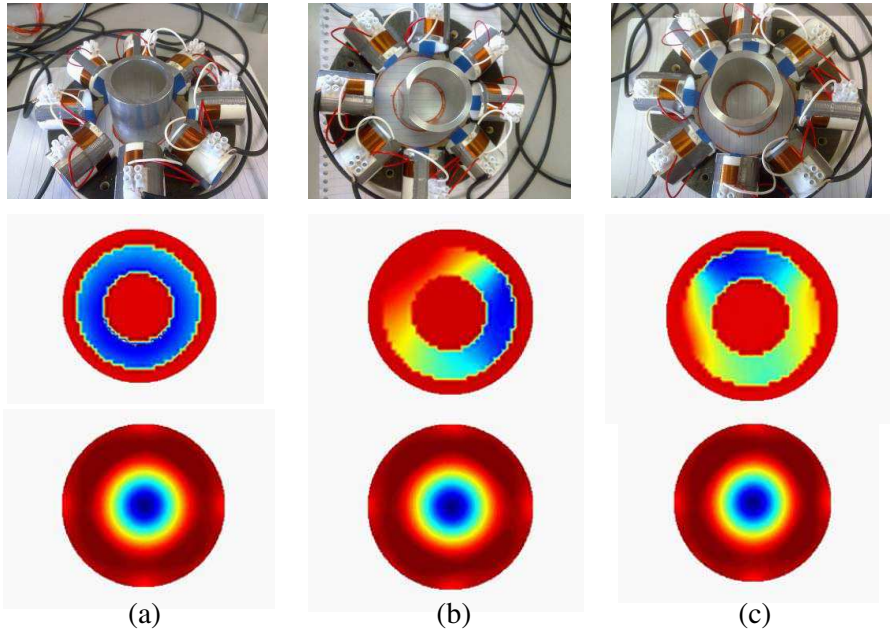


Figure 9. Pipes imaging with different conditions. Top row is the true samples, middle row shows the NPFM results, and the bottom shows the PBRM results. (a) Full pipe. (b) One big cut. (c) One big and one small cut.

To better understand the challenging aspects of the tests of Figure 9, the measured voltages and voltage differences are shown in Figure 10. Figure 10(a) shows the absolute voltage measured from a full pipe. The reference data for a full pipe were measured data in free space so the images of Figure 9(a) are produced using these reference data. Figure 10(b) shows the differences between the full pipe data and the pipe with one and two cuts. The images of Figures 9(b) and 9(c) are generated by considering full pipe as a reference data. In the case of Figures 9(b) and 9(c) as well as Figure 6, it appears that when the full pipe was chosen as reference, the signature of cuts (and opening in case of Figure 6) were clearer than if the free space background was chosen as a reference. This suggests that the measurement of full pipe acts as an additional calibration and further enhances our NPFM results. The choice of reference data in this case is a trade off between nonlinearity error (which is the case for free space background) and smaller measured voltage (which is the case for full pipe as background as shown in Figure 10(b)). It appears that

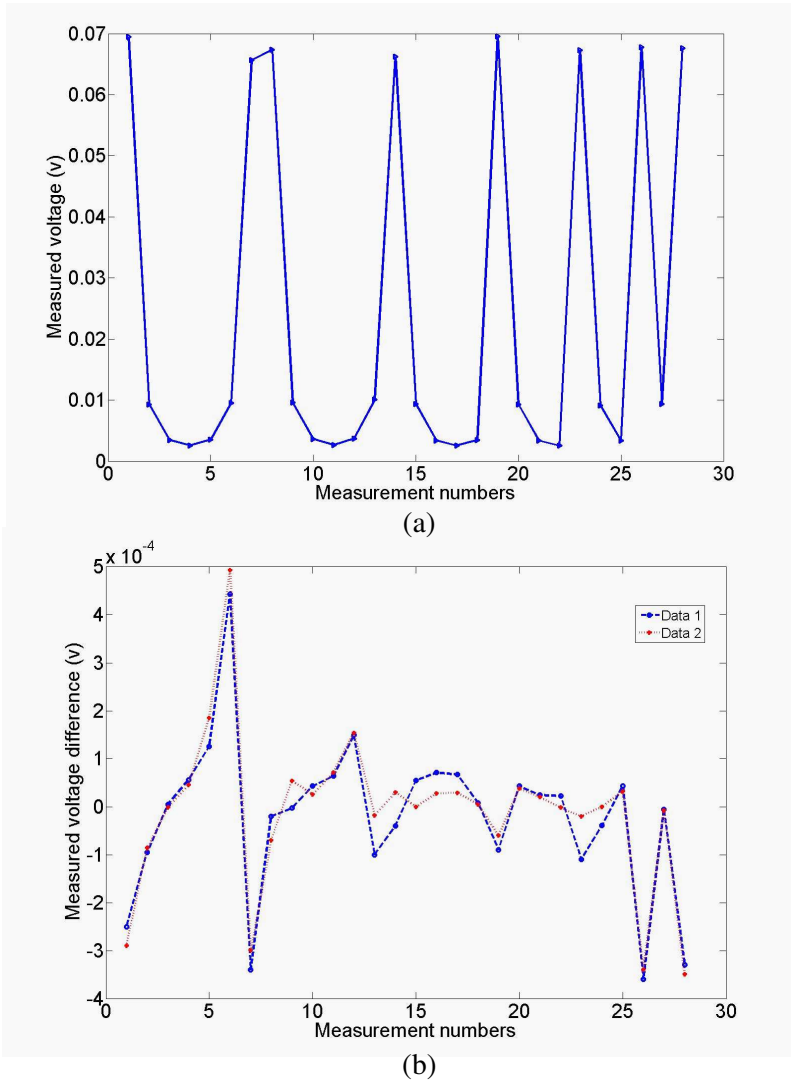


Figure 10. (a) Absolute induced voltage for full pipe of the Figure 8(a). (b) Voltage difference between full pipe and pipe with cuts (Data 1: voltage difference between full pipe and pipe with one large cut of Figure 8(b), and Data 2: voltage differences between full pipe and pipe with two cuts in Figure 8(c)).

the nonlinearity is a more significant error here. To maintain the capability of rapid inspection using linear reconstruction algorithm we recommend the calibration against full pipe. In all cases, the PBRM has failed to show the damages in the pipe, and the proposed NPFM shows superior performance. The voltage differences in our test experiments are small but still in range of microvolt and are measurable. Detection of smaller cut (1.5 mm in an imaging region of 100 mm) shows that a significant improvement in information can be extracted from the MIT system.

5. CONCLUSION

Experimental outcome has shown the improvement of the MIT imaging for pipeline application. The results confirm the MIT imaging as a promising tool for inspection of metallic pipelines. The NPFM enables the system to produce better results taking advantage of *a priori* knowledge of the pipe geometry. The results presented in this paper are laboratory-based experiments; further work is needed to apply the method in real industrial applications. The industrial pipelines are coated with claddings, normally non-conductive. A cladding with a layer of conductor will pose a challenge to the electromagnetic imaging method proposed here. In the future work, a three dimensional system will be set up, and the existing eight channels will be upgraded to sixteen channels for better resolution. As an expansion of this work, we will further investigate the possibility of using the proposed method to detect the internal surfaces of the metallic pipes. It is well known that using traditional PBRM, a resolution of around 10% of radius of coil array can be achieved. Using the proposed NPFM, we have shown that much better resolution can be achieved for the particular case of the pipe geometry.

REFERENCES

1. Griffiths, H., "Magnetic induction tomography," *Meas. Sci. Technol.*, Vol. 12, 1126–1131, Dec. 2001.
2. Dyck, D. N., D. A. Lowther, and E. M. Freeman, "A method of computing the sensitivity of the electromagnetic quantities to changes in the material and sources," *IEEE Trans. on Magn.*, Vol. 3, No. 5, Sep. 1994.
3. Ktistis, C., D. W. Armitage, and A. J. Peyton, "Calculation of the forward problem for absolute image reconstruction in MIT," *Physiol. Meas.*, Vol. 29, S455–S464, 2008.

4. Peyton, A. J., Z. Z. Yu, and G. M. Lyon, "An overview of electromagnetic inductance tomography: Description of three different systems," *Meas. Sci. Technol.*, Vol. 7, No. 3, 261–271, Mar. 1996.
5. Korjenevsky, A., V. Cherepenin, and S. Sapetsky, "Magnetic induction tomography: Experimental realization," *Physiol. Meas.*, Vol. 21, No. 1, 89–94, 2000.
6. Scharfetter, H., K. Helmut Lackner, and J. Rosell, "Magnetic induction tomography: Hardware for multi-frequency in biological tissue," *Physiol. Meas.*, Vol. 22, No. 1, 131–146, Feb. 2001.
7. Ma, X., A. J. Peyton, S. R. Higson, A. Lyons, and S. J. Dickinson, "Hardware and software design for an electromagnetic induction tomography (EMT) system applied to high contrast metal process applications," *Meas. Sci. Technol.*, Vol. 17, No. 1, 111–118, 2006.
8. Coveney, J. A., M. H. Pham, A. K. Kyllö, and N. B. Gray, "Comparison of modeling approaches for the eddy current problem as applied to the geometry of a taphole," *Meas. Sci. Technol.*, Vol. 17, No. 2, 340–352, 2006.
9. Hansen, P. C., "Rank-deficient and discrete ill-posed problems: Numerical aspects of linear inversion," *Society for Industrial and Applied Mathematics*, Philadelphia, 1998.
10. Soleimani, M. and W. R. B. Lionheart, "Image reconstruction in three-dimensional magnetostatic permeability tomography," *IEEE Trans. on Magn.*, Vol. 41, No. 4, 1274–1279, 2005.
11. Soleimani, M., "Sensitivity maps in three-dimensional magnetic induction tomography," *Insight*, Vol. 48, No. 1, 39–44, 2006.
12. Wei, H.-Y. and M. Soleimani, "Three-dimensional magnetic induction tomography imaging using a matrix free Krylov subspace inversion algorithm," *Progress In Electromagnetics Research*, Vol. 122, 29–45, 2012.
13. Soleimani, M., "Simultaneous reconstruction of permeability and conductivity in magnetic induction tomography," *Journal of Electromagnetic Waves and Applications*, Vol. 23, Nos. 5–6, 785–798, 2009.
14. Soleimani, M., C. N. Mitchell, R. Banasiak, R. Wajman, and A. Adler, "Four-dimensional electrical capacitance tomography imaging using experimental data," *Progress In Electromagnetics Research*, Vol. 90, 171–186, 2009.
15. Banasiak, R., R. Wajman, D. Sankowski, and M. Soleimani, "Three-dimensional nonlinear inversion of electrical capacitance tomography data using a complete sensor model," *Progress In*

- Electromagnetics Research*, Vol. 100, 219–234, 2010.
16. Goharian, M., M. Soleimani, and G. R. Moran, “A trust region subproblem for 3D electrical impedance tomography inverse problem using experimental data,” *Progress In Electromagnetics Research*, Vol. 94, 19–32, 2009.
 17. Catapano, I., F. Soldovieri, and L. Crocco, “On the feasibility of the linear sampling method for 3D GPR surveys,” *Progress In Electromagnetics Research*, Vol. 118, 185–203, 2011.
 18. Flores-Tapia, D., M. O’Halloran, and S. Pistorius, “A bimodal reconstruction method for breast cancer imaging,” *Progress In Electromagnetics Research*, Vol. 118, 461–486, 2011.
 19. Asimakis, N. P., I. S. Karanasiou, and N. K. Uzunoglu, “Non-invasive microwave radiometric system for intracranial applications: A study using the conformal L-notch microstrip patch antenna,” *Progress In Electromagnetics Research*, Vol. 117, 83–101, 2011.